American Journal of
Polymer Science & Engineering
http://www.ivyunion.org/index.php/ajpse/index
Vol 2, Article ID 201400573, 17 pages

American Journal of
Polymer Science & Engineering

Research Article

Novel Nanofiltration Membranes of Poly(4-Chlorostyrene)-grafted-1-(4-thiocarbamoylaminophenyl-sulfonylphenyl)thiourea and Gold/Polystyrene Composite Nanoparticle

Ayesha Kausar

Nanosciences and Catalysis Division,National Centre For Physics, Quaid-i-Azam University Campus, Islamabad, Pakistan.

Abstract

In the current research poly(4-chlorostyrene) grafted with thiourea-based diamine (1-(4-thiocarbamoylaminophenylsulfonylphenyl) thiourea) (PCS-g-DA) was prepared. The nanofiltration membrane of PCS-g-DA was prepared using tetrahydrofuran as solvents *via* phase inversion method. For the reinforcement purpose gold nanoparticles and its composite nanoparticles with polystyrene microspheres (AuNPs-PSNPs) have been designed and studied using transmission electron microscopy. Cross-section and internal fractured PCS-g-DA/AuNPs-PSNPs membrane surfaces were characterized by scanning electron microscopy. Nanoporous membrane morphology was observed at increased nanofiller loading. The membrane property study revealed higher pure water permeation flux, recovery and solute rejection for membranes with higher AuNPs-PSNPs content. The PCS-g-DA/AuNPs-PSNPs membrane with 1 wt. % loading showed flux of 17.4 $mLcm^{-2}$ min^{-1} and salt rejection ratio of 72.2 %. In addition glass transition temperature, porosity, and water uptake of membranes were increased with filler loading. The tensile strength was increased from 29.5-37.6 MPa in PCS-g-DA/AuNPs-PSNPs 0.1-1 membranes. Efficiency of the gold/polystyrene nanoparticles reinforced membranes was found to be 99 % for the removal of Hg^{2+} and Pb^{2+}. According to the results, the composite membranes have fine nanofiltration characteristics to be utilized in advance water treatment industrial units.

Keywords: Nanofiltration; poly(4-chlorostyrene); morphology; tensile strength; flux

Academic Editor: Taihong Shi, PhD, PhD, Sun Yat-sen University, China

Received: November 21, 2014; **Accepted**: December 28, 2014; P**ublished**: January 26, 2015

Competing Interests: The authors have declared that no competing interests exist.

***Correspondence to**: Ayesha Kausar, Nanosciences and Catalysis Division, National Centre For Physics, Quaid-i-Azam University, Islamabad, Pakistan; Email: asheesgreat@yahoo.com

1. Introduction

Membrane is a selective and permeable barrier between two phases that speed up the separation of the constituents when external force is applied [1-3]. Depending on the charge and size of solutes to be separated, the process can be categorized as reverse osmosis, ultrafiltration, microfiltration or nanofiltration. Among these processes, nanofiltration (NF) has been focused due to fine separation features compared with reverse osmosis and ultrafiltration [4-7]. NF usually involves the separation of organic solutes or monovalent and divalent salts having molecular weight in the range of 200 to 1000 g/mol [8]. However the commercial polymeric NF membranes are suitable for treating aqueous streams at pH 2-10. Several potential applications in the industry involve much more aggressive conditions [9]. The advancement of nanofiltration technology in separation processes is being widely studied owing to its benefits such as high flux, low operation pressure, and high retention offered by organic molecules and multivalent anionic salts [10]. Mostly the nanofiltration membranes developed up to now are the composite membranes having a selective layer on top of the micro-porous substrate. The selection of membrane material depends on both the physical and chemical compatibility of the selective layer with the substrate, which in turn determines the stability and performance of the resulting composite membranes [11, 12]. Researchers have focused various approaches for the fabrication of composite NF membranes such as dip coating method, vacuum coating process, plasma initiated polymerization, vapor deposition, photo-initiated polymerization, electron beam irradiation, resin-filled chelating, atom transfer radical polymerization, and *in-situ* amines cross-linking [13-15]. In this regard, polyvinyl alcohol/polysulfone hollow fiber NF membranes have been fabricated [16]. Polyvinyl chloride (PVC) has been employed as an important matrix for NF membranes. PVC and chlorinated-PVC have been used to engineer membranes with fine antifouling behavior and protein dismissal ratios [17]. In an alternative effort, PVC-based NF membrane was prepared through phase inversion process [18]. Most of the developing countries suffer from lack of pure water as well as excessive salinity in the water ways. One of the recommendations and proposals for resolving this problem is to build water salt elimination set-ups. One of the interesting application areas of noble metal nanoparticles is the removal of heavy metals from drinking water. The functionalized noble metal nanoparticles have the potential for the detection and removal of heavy metals. For this purpose heavy metal specific biomolecule functionalized gold nanoparticles have been utilized. In a similar approach, the peptide-functionalized gold nanoparticles were utilized for the colorimetric detection of Hg^{2+} and Pb^{2+} at ppb level [19].

The preparation of hybrid nanofiltration membrane has relatively less investigated compared with other membranes in water treatment technology. The hybrid nanofiltration seems to be a suitable method for the removal of hardness, sulfates, chlorides, and bacteria in a single-step from ground water. The type and concentration of nanofiller are the most important parameters in determining the membrane morphology and performance. In this research work, poly(4-chlorostyrene) was grafted with a novel thiourea-based diamine i.e. 1-(4-thiocarbamoylaminophenyl-sulfonylphenyl)thiourea. The nanofiltration membranes of poly(4-chlorostyrene)-*grafted*-1-(4-thiocarbamoylaminophenyl-sulfonylphenyl)thiourea (PCS-g-DA) were then prepared using phase inversion technique. The exchange of solvent and non-solvent plays significant role in this regard. Our motivation to utilize functional polystyrene matrix in preparing the filtration membrane actually stems from the unique properties of the matrix when grafted with a novel diamine. The presence of thiourea functionality in membrane material would induce hydrophilicity, which may ensure high water permeation and impede bio-fouling/shrinkage because of the low interfacial energy between a surface

and water. To enhance the interfacial compatibility between poly(4-chlorostyrene) and nanofiller, we also prepared modified composite nanofiller. Another novel aspect of current research was therefore the preparation of gold/polystyrene composite nanoparticle (AuNPs-PSNPs). The noble metal nanoparticles were introduced as reinforcement to remove several toxic metal ions from water. Consequently, effect of the addition of nanofiller content on the performance and structure of novel membrane was investigated using relevant methods and techniques.

2. Experimental

2.1. Materials

Poly(4-chlorostyrene) (M_w~75,000) was purchased from Aldrich. Styrene (≥99 %), obtained from Aldrich was purified by distillation under reduced pressure. Poly(vinylpyrrolidone) (PVP K-30) was purchased from Acros Organics. $HAuCl_4$ (10 nm particle size), 2-2'-azoisobutyronitrile (AlBN, ≥98 %), 4-(4-aminophenylsulfonyl)benzenamine (APSBA) (97%), ammonium thiocyanate (98%), and sodium carbonate were obtained from Aldrich and used as received.

2.2. Characterization Techniques

The infrared (IR) spectra were recorded using a Fourier transform infrared (FTIR) Spectrometer, Model No. FTSW 300 MX, manufactured by BIO-RAD, California, USA (4 cm^{-1} resolution). The SEM images were obtained by Scanning Electron Microscope S-4700 (Japan Hitachi Co. Ltd.) and TEM images were taken by Transmission Electron Microscope H-800 (Japan Hatachi Co. Ltd). The particle size and the particle size distribution were measured by Zetasizer Nano ZS particle analyzer (UK Malvern Instruments Ltd.) in the means of dynamic light scattering (DLS). The tensile tests were conducted on dog-bone-shape samples using Testomeric materials testing machine M500–30CT at a speed of 500 mm/min (ASTM D412). The glass transition was measured using Perkin-elmer DSC-2C differential scanning calorimeter in N_2 gas flow at a heating rate of 10 ℃/min. To analyze the water content, membranes were soaked in distilled water for 24 h. The wet membranes were first kept at 100 ℃ for 24 h, and subsequently weighed to obtain the dry weight. The percent solvent content was calculated using the following equation:

$$\% \text{ Solvent Content} = \frac{W_1 - W_2}{W_2}$$

Where:

W_1 = Wet membrane weight (g)
W_2 = Dry membrane weight (g)

To analyze the membrane porosity, the samples were soaked in distilled water for 24 h. The membranes were dried at 100 ℃ for 24 h and weighed. Porosity was calculated using the following equation:

$$\text{Porosity} = \frac{W_1 - W_2}{A_h}$$

Where:

W_1 = Wet membrane weight (g)
W_2 = Dry membrane weight (g)
A_h = Membrane area (cm^2)

The pure water flux of membrane was measured using membrane cell with cross-flow mode. The permeate was collected every 10 min for 1 h. The membranes after compaction were subjected to pure water flux estimation at trans-membrane pressure of 345 kPa. The permeability was measured under steady state flow. Pure water flux was calculated as follows:

$$J_w = \frac{Q}{At}$$

Where:

Q = Quantity of permeate collected (L)
J_w = Pure water flux ($mLcm^{-2}\ min^{-1}$)
A = Membrane area (cm^{-2})
t = Sampling time (min)

The length and the width of a piece of wet membrane were measured using a vernier caliper. Then the membrane was heated at 100 ℃ for 24 h. The length and the width of the dry membrane sample was also measured. The shrinkage ratio was calculated using the equation:

$$\text{Shrinkage ratio} = \left[1 - \left(\frac{ab}{a_o b_0}\right)\right].100$$

Where:

A = length of dry membrane (m)
b = breadth of dry membrane (m)
a_o = length of wet membrane (m)
b_o = breadth of wet membrane (m)

Rejection indicates the amount of components rejected by membranes. It shows the separation efficiency of the components by the membrane. It is calculated as:

$$R_e = 1 - \frac{Cp}{Cf}$$

Where:

Re = Rejection

Cp = Concentration of components in permeate (g/m^3)

Cf = Concentration of components in feed water (g/m^3)

Recovery is also known as productivity. Here also the membrane cell with cross-flow mode was used. According to mass balance, the feed flow is equal to the sum of concentrate flow and permeates flow. Recovery was calculated by:

$$\gamma = \frac{Qp}{Qf} . 100$$

Where:

γ = Recovery (%)

Qp = Permeate flow (m^3/h)

Qf = Feed flow (m^3/h)

The solid-liquid extraction tests of nitrates or chloride salts of Fe^{3+}, Co^{2+}, Ni^{2+}, Cu^{2+}, Cd^{2+}, Pb^{2+} and Hg^{2+} were carried out using neat PCS-*g*-DA and PCS-*g*-DA/AuNPs-PSNPs 1 membrane. After filtration, the concentration of each cation in the liquid phase was determined by inductively coupled plasma mass spectrometry (ICP-MS, Agilent 7500). Consecutive dilutions of sample aliquots with ultra-pure water/nitric acid (5% v/v) were performed to reach concentrations in the range of the calibration curve (0 to 40 ppb), thus direct information regarding the extraction percentages of metal ions was obtained. The effectiveness of membranes for the extraction of environmentally toxic heavy metal ions was also studied in terms of distribution coefficient (*Kd′*) and solid-liquid extraction selectivity ($\alpha_{S,L}$) [20]. Accordingly, *Kd′* is the measure of the capacity of material to extract cations under competitive conditions, where *%E is* extraction percentage; *V* is volume of the solution (liters) and *n* the molar amount of polymer structural units.

$$Kd' = \left(\frac{\%E}{100 - \%E}\right)\left(\frac{V}{n}\right)$$

$\alpha_{S,L}$ is the ratio of two distribution coefficients. Hg^{2+} cation was taken as the reference, as it has the highest distribution coefficient (Kd'_{M2}).

$$\alpha_{S,L} = \frac{Kd_{M1}}{Kd_{M2}} = \frac{Kd'_{M1}}{Kd'_{M2}}$$

2.3. Synthesis of polystyrene microspheres (PSNPs)

For the synthesis of PSNPs, 2.6 g of PVP stabilizer was dissolved in 160 mL of 2-propanol at 70 ℃. 0.2 g of AIBN initiator was dissolved in 20 g of styrene and added to the above mixture. The polymerization was allowed to proceed at 70 ℃ for 24 h. Subsequently, the PS microspheres were centrifuged for 6h and washed with ethanol and deionized water [21].

2.4. Synthesis of gold nanoparticles-coated polystyrene nanocomposite particles (AuNPs-PSNPs)

0.025 g of Na_2CO_3 was dissolved in 100 mL of deionized water. The solution was added to 16.4 mL of $HAuCl_4$ aqueous solution (3×10^{-3} M) and stirred for 0.5 h. Then 0.1 g of PS (10 wt. %) emulsion and 0.25 mL of formaldehyde (35 wt. %) were added to the above mixture and stirred for 1 h. The resulting AuNPs-PSNPs nanoparticles were separated out by centrifugation. The nano-particles were re-dispersed in ethanol and deionized water and separated out by centrifugation.

2.5. Synthesis of 1-(4-thiocarbamoylaminophenylsulfonylphenyl)thiourea (TCAPST)

4-(4-aminophenylsulfonyl)benzenamine (0.2 mol), concentrated HCl (16 mL), ammonium thiocyanate (0.2 mol) and deaerated water (120 mL) were mixed and heated on a steam bath for 2 h. The mixture was allowed to cool to room temperature. Afterwards the mixture was gradually evaporated to dryness for 6-7 h. The product obtained was boiled with charcoal in ethanol, filtered, and cooled. 1-(4-thiocarbamoylaminophenyl-sulfonylphenyl)thiourea was recrystallized from ethanol and dried under vacuum at 90 ℃ for 36 h [22]. Elemental analysis for $C_{14}H_{14}N_4O_2S_3$: Calculated = % C 45.88, % H 3.85, % N 15.29; Found = %C 43.32, %H 3.69, %N 14.49. FTIR (KBr): 3365 cm^{-1}, 3234 cm^{-1} (N–H stretch), 3019 cm^{-1} (aromatic C–H stretch), 2945 (aliphatic C–H stretch), 1599 cm^{-1} (N–H bend), 1413 cm^{-1} (C–N stretch), 1301 and 1157 (S=O stretch), 1123 cm^{-1} (C=S stretch).

2.6. Preparation of the hybrid membranes

A homogenous solution of poly(4-chlorostyrene) matrix (1 g) was first prepared in 10 mL of THF. 10 wt. % of (1-(4-thiocarbamoylaminophenyl-sulfonylphenyl)thiourea) was added to the matrix (Fig. 1). The mixture was refluxed at 80 ℃ for 2 h. The desired amount of AuNPs-PSNPs (0.1-1 wt. %) was then added to the above mixture and reaction flask was transferred to ultrasonic bath cleaner for 6 h. The obtained homogeneous solutions were cast onto glass plates using casting knife. After 0.5 h, the films prepared were dipped into deionized water as non-solvent. In this step, the exchange of solvent and non-solvent led to the membrane formation. After phase separation step and membrane formation, the membranes were kept in deionized water for 24 h to remove the remaining solvent. Finally the membranes were dried at 60 ℃ for 24 h [23]. The membrane properties were measured using the experimental nanofiltration set-up (Fig. 2).

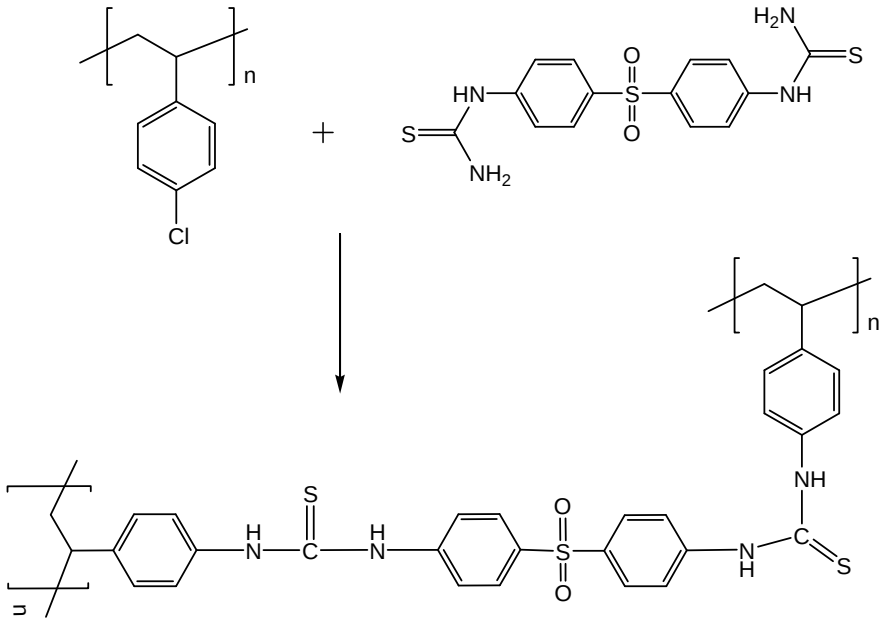

Figure 1 Schematic illustration for the formation of poly(4-chlorostyrene)-*grafted*-diamine.

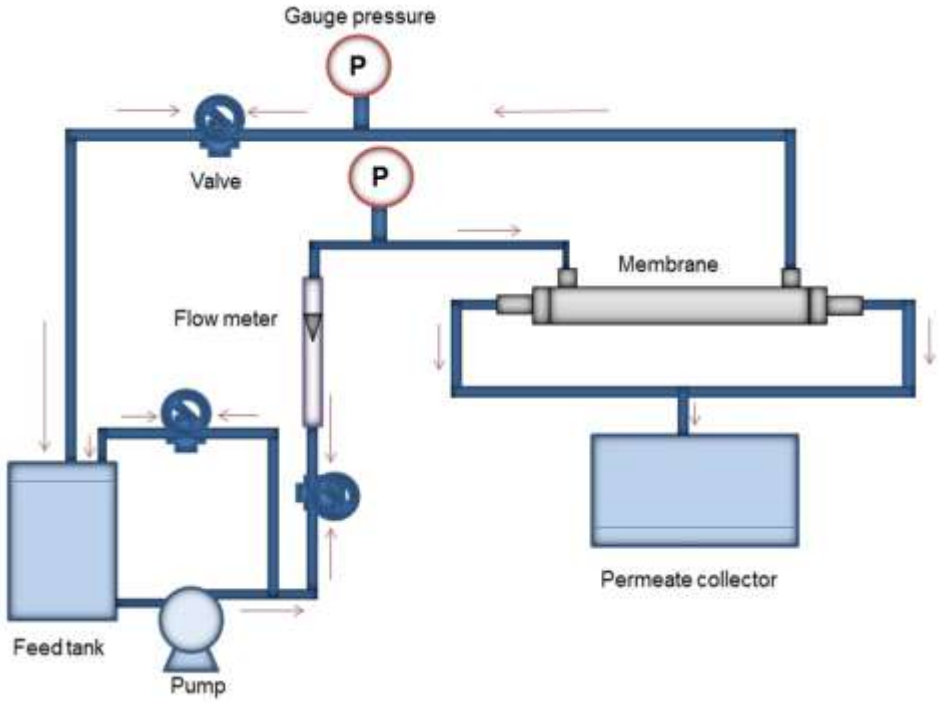

Figure 2 Experimental nanofiltration setup.

3. Result and Discussion

3.1. Mechanical features

Effect of gold/polystyrene nanoparticle reinforcement (0.1 to 1 wt. %) on the properties of cross-linked matrix was investigated. According to the tensile results (Fig. 3 and Table 1), there was remarkable improvement in the mechanical properties of PCS-g-DA/AuNPs-PSNPs 0.1-1 membranes. On the whole, tensile stress, tangent modulus, and toughness were increased upon the nanofiller addition. On the other hand, the elongation at break was decreased with the addition of different amount of reinforcement. Increasing the nanofiller content from 0.1 to 1-wt. % decreased the elongation at break from 5.2 to 3.7 %. The tensile strength of unfilled PCS-g-DA matrix was found to be lower (27.7 MPa) compared with the hybrids. The most probable reason was the strain-induced crystallization of matrix due to cross-linking. The membranes filled with AuNPs-PSNPs nanoparticles revealed enhancement in tensile strength, modulus, and toughness. The higher nanoparticle content provided much more interface for polymer chains compared with that of lower loading level. The enhancement in the tensile properties was therefore notable due to good compatibility of nanoparticles with matrix [24]. The tensile strength was found higher for PCS-g-DA/AuNPs-PSNPs 1 hybrid with 1 wt. % filler content (37.6 MPa) relative to PCS-g-DA/AuNPs-PSNPs 0.1-0.5 composites (29.5-31.5 MPa) and pristine matrix. Similar increasing trend was found for the tensile modulus of nanocomposites. The tensile modulus of PCS-g-DA/AuNPs-PSNPs 1 (2.5 GPa) was found to be higher than PCS-g-DA/AuNPs-PSNPs 0.1 (1.3 GPa), PCS-g-DA/AuNPs-PSNPs 0.3 (1.8 GPa) and PCS-g-DA/AuNPs-PSNPs 0.5 (2.1 GPa) and neat matrix (1.1 GPa). The toughness of the materials also increased due to the fact that better compatiblized materials are tougher. The addition of AuNPs-PSNPs revealed an enhancement in rigidity from 234 to 589 Jm^{-3}. The toughness of the composites was also higher relative to base matrix (34 Jm^{-3}). The physical adhesion between the nanofiller particles and matrix operated as a key factor in enhancing the tensile characteristics.

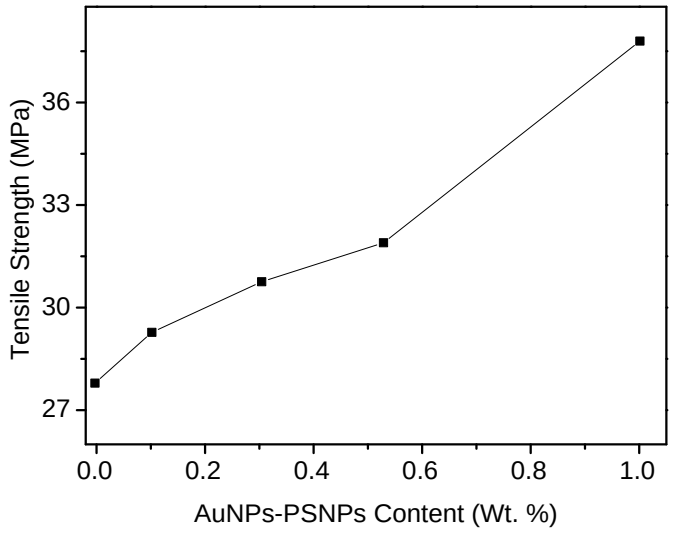

Figure 3 Drift of tensile strength *vs.* AuNPs-PSNPs in PCS-g-DA/AuNPs-PSNPs membranes.

Table 1 mechanical property of PCS-*g*-DA and PCS-*g*-DA/AuNPs-PSNPs membranes.

Composition	Tensile Strength (MPa) ± 0.02	Elongation at break ± 0.01 (%)	Tensile Modulus (GPa) ± 0.03	Toughness (Jm^{-3}) ± 0.02
PCS-g-DA	27.7	1.2	1.1	34
PCS-g-DA/AuNPs-PSNPs 0.1	29.5	5.2	1.3	234
PCS-g-DA/AuNPs-PSNPs 0.3	30.6	4.9	1.8	367
PCS-g-DA/AuNPs-PSNPs 0.5	31.5	4.1	2.1	477
PCS-g-DA/AuNPs-PSNPs 1	37.6	3.7	2.5	589

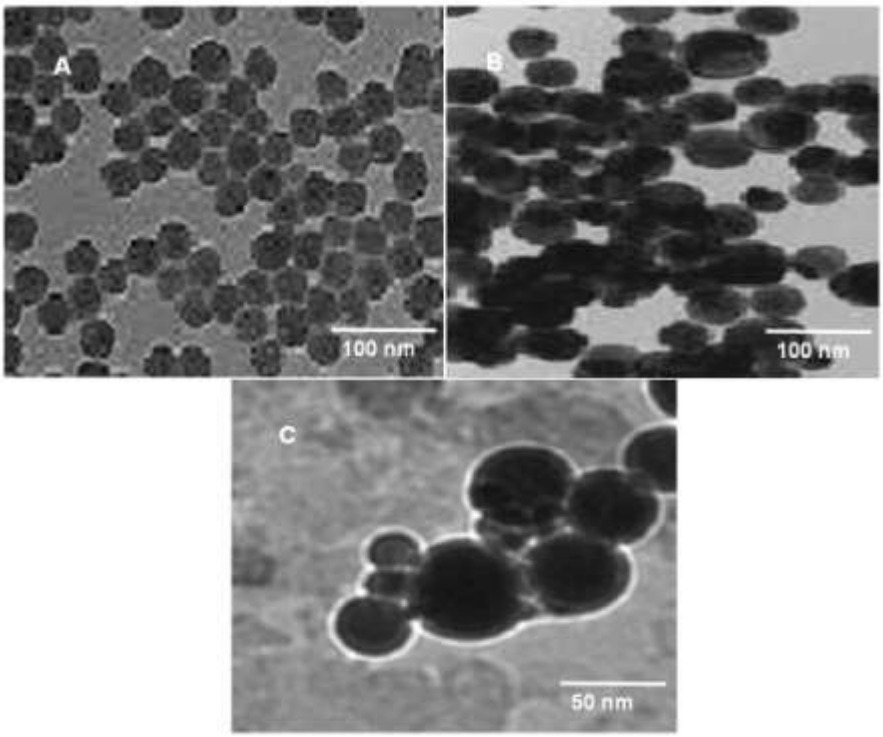

Figure 4 TEM micrographs of (A) AuNPs at 100 nm; (B) AuNPs-PSNPs at 100 nm; (C) AuNPs-PSNPs at 50 nm.

3.2. Morphological Investigation

TEM image of gold nanoparticles depicted spherical shape and homogeneous distribution (Fig. 4 A). The AuNPs were analyzed with Zetasizer Nano ZS particle analyzer and found to have size of 10-20 nm. Fig. 4 B & C show the morphology of polystyrene nanoparticles grafted with gold nanoparticles. According to the results, the AuNPs-PSNPs composite nanoparticles also took rotund shape in the size range of 30-50 nm with a narrow distribution. The high specific surface area of nanoparticles provide sufficient inter-phase for the polymer/filler interaction. Thus the well-oriented polymer segments with the neighboring filler particles may bear the outer force concurrently. As a result, the inside details turned out to be higher strength and modulus as shown by tensile results presented in the preceding section. FESEM images of PCS-*g*-DA/AuNPs-PSNPs 0.1, PCS-*g*-DA/AuNPs-PSNPs 0.3 and PCS-*g*-DA/AuNPs-PSNPs 0.5 are given in Fig. 5 A-F.

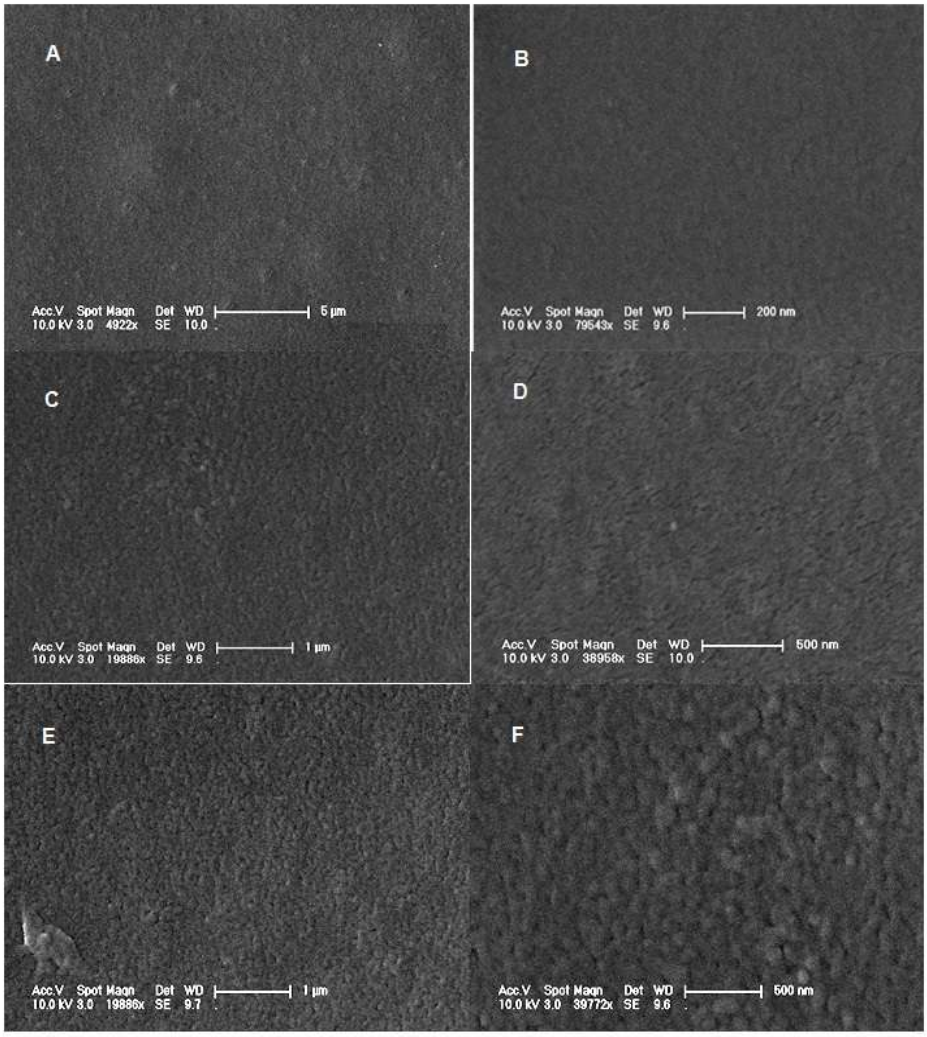

Figure 5 FESEM micrographs of (A) PCS-*g*-DA/AuNPs-PSNPs 0.1 at 5 µm; (B) PCS-*g*-DA/AuNPs-PSNPs 0.1 at 200 nm; (C) PCS-*g*-DA/AuNPs-PSNPs 0.3 at 1 µm; (D) PCS-*g*-DA/AuNPs-PSNPs 0.3 at 500 nm; (E) PCS-*g*-DA/AuNPs-PSNPs 0.5 at 1 µm; (F) PCS-*g*-DA/AuNPs-PSNPs 0.5 at 500 nm.

The PCS-*g*-DA/AuNPs-PSNPs 0.1 with 0.l wt. % AuNPs-PSNPs revealed porous morphology but the nanopores were smaller in size and hardly visible at 200 nm (Fig. 5 B). Micrographs in Fig. 5 C & D also showed slightly porous morphology for PCS-*g*-DA/AuNPs-PSNPs 0.3 with higher nanoparticle loading level. However, the granular and porous morphology was observed with the increased filler loading of 0.5 wt. % in PCS-*g*-DA/AuNPs-PSNPs 0.5 (Fig. 5 E & F). The cross-section morphology PCS-*g*-DA/AuNPs-PSNPs 1 membrane showed sponge-like micropores (Fig. 6 A). Furthermore, the increase of nanopores was obvious in Fig. 6 B-D relative to PCS-*g*-DA/AuNPs-PSNPs 0.1-0.5. Generally the appropriate porosity is necessary to enhance the filtration efficiency of the membranes [25]. However, very high porosity and larger pores will adversely impact the membrane performance because pores cannot be closed effectively and the membrane tends to shrink. The morphological variation was quite apparent in PCS-*g*-DA matrix with composite nanoparticle addition owing to better polymer/filler interaction in PCS-*g*-DA/AuNPs-PSNPs 0.1-1 membranes.

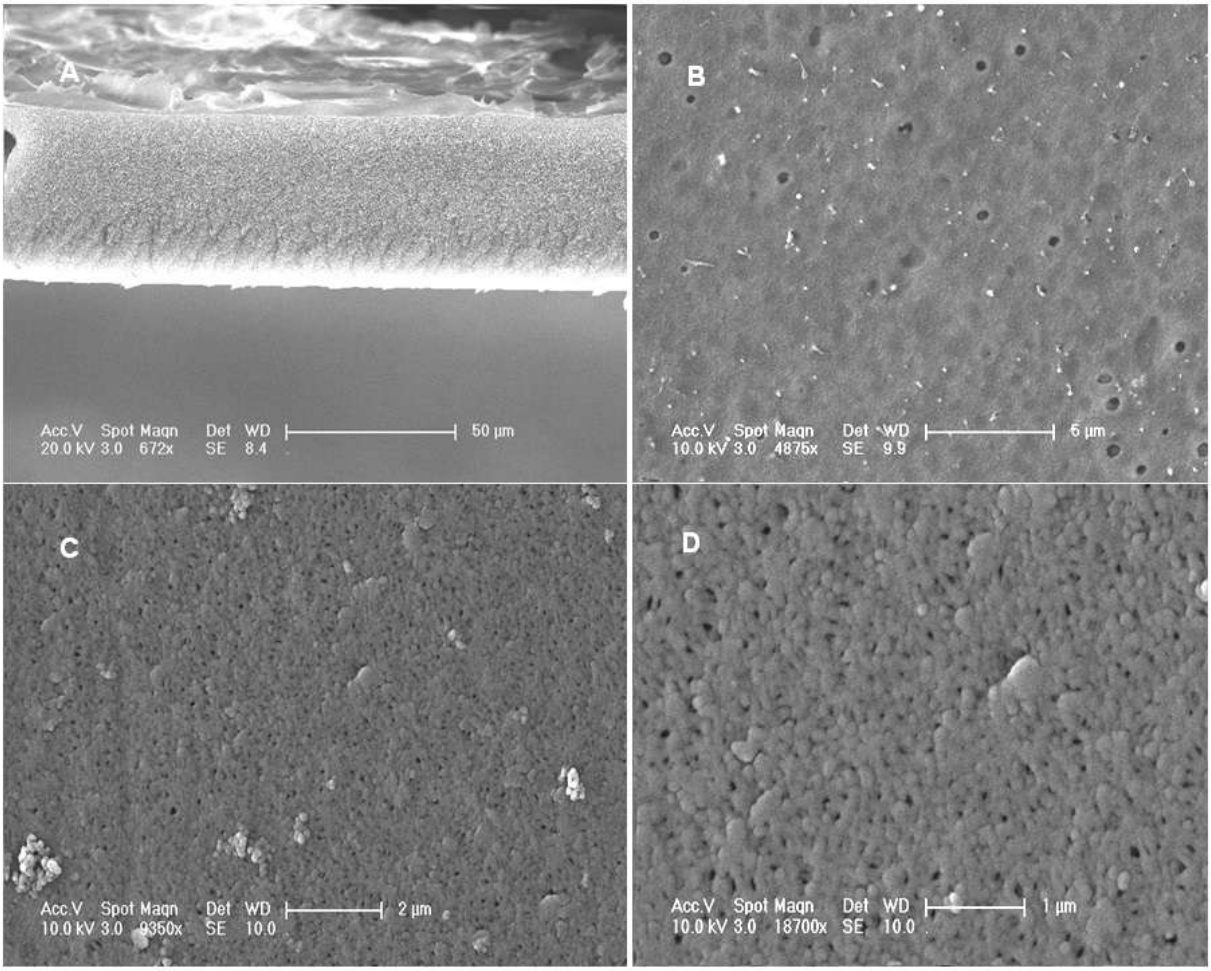

Figure 6 FESEM micrographs of (A) PCS-*g*-DA/AuNPs-PSNPs 1 at 50 µm; (B) PCS-*g*-DA/AuNPs-PSNPs 1 at 5 µm; (C) PCS-*g*-DA/AuNPs-PSNPs 1 at 2 µm; and (D) PCS-*g*-DA/AuNPs-PSNPs 1 at 1 µm.

3.3. Membrane properties and performance

Membrane properties and performance were evaluated through % porosity, % solvent content, shrinkage ratio, flux, recovery, and salt rejection tests. The porosity measurement of PCS-g-DA and PCS-g-DA/AuNPs-PSNPs 0.1-1 membranes is given in Table 2. Neat PCS-g-DA membrane had lower porosity ~ 0.11 g/cm^2 in water and among all the solvents tested. The membranes showed steady increase in porosity with nanofiller content in different solvents (water, ethanol, methanol and propanol). The reason was the increase in the hydrophilic nature of the membranes because of the nanofiller addition. Similarly the porous nature of the membranes was decreased as the hydrophilicity of solvent decreased (moving from water to propanol). Secondly, to access the hydrophilic nature of the membranes, % solvent content of membranes was also measured (Table 3). % Solvent content was found to demonstrate increasing tendency with composite nanoparticle loading in all solvents. Both the porosity and % solvent content of the membranes were maximum for PCS-g-DA/AuNPs-PSNPs 1 and was detected minimum for neat PCS-g-DA. However, similar to the porosity, % solvent content was also observed to decline when moving from water to less polar solvent. The porosity (water) and % water content of PCS-g-DA/AuNPs-PSNPs 1 were found to be 0.29 g/cm^2 and 3.17 % respectively. In addition, higher porosity of PCS-g-DA/AuNPs-PSNPs 1 resulted in lower shrinkage ratio of the membrane. Table 4 shows that as the AuNPs-PSNPs filler content increased from 0.1-1 wt. %, the shrinkage ratio was decreased. Due to increase in the nanoporous nature of the membranes shrinkage ratio was decreased from 10.2 to 8.12 (water). The Measurement of pure water flux was an important nanofiltration membranes characteristic. The water flux was expected to increase with because of higher membrane porosity, % solvent content and hydrophilicity. Accordingly PCS-g-DA/AuNPs-PSNPs 1 membrane showed higher water flux of 17.4 mLcm^{-2} min^{-1} (Table 5). The water flux of PCS-g-DA, PCS-g-DA/AuNPs-PSNPs 0.1, PCS-g-DA/AuNPs-PSNPs 0.3 and PCS-g-DA/AuNPs-PSNPs 0.5 membranes were found to be lower around 14.2, 14.9, 15.7 and 16.2 mLcm^{-2} min^{-1} respectively. Moreover the salt (NaCl) rejection ratio of the membrane with higher filler loading was found to be higher (72.2 %) compared with 0.1 wt. % loading (52.7 %). The membrane recovery of PCS-g-DA/AuNPs-PSNPs 1 was also maximum ~ 87.2 %. The over all performance of 1 wt. % filler loaded PCS-g-DA/AuNPs-PSNPs membrane was evaluated as most favorable to be used in water purification systems [25].

3.4. Extraction of toxic metal ions

In addition to the gold/polystyrene nanoparticles, the thiourea moieties were introduced in the cross-linked matrix. Thiourea group also acts as host unit for both cations and anions. Thiourea-based materials have been designed for the extraction of salts through ion-dipole interaction [26, 27]. The membranes were tested in terms of distribution coefficient (*Kd*′) and solid-liquid extraction selectivity ($\alpha_{S,L}$) [20, 28]. Table 6 presents the solid-liquid extraction results for the removal of several cations from aqueous solution using PCS-*g*-DA and PCS-*g*-DA/AuNPs-PSNPs 1 membarens. The % E of PCS-*g*-DA/AuNPs-PSNPs 1 membrane was found up to 67 % for the extraction of Fe^{3+}, Co^{2+}, Ni^{2+}, Cu^{2+}, and Cd^{2+}. The extraction efficiency of the membranes was 100 % for Pb^{2+} and Hg^{2+} due to the combined effect of thiourea moieties and gold nanoparticles in the removal of heavy metal ions [29]. The extraordinarily high extraction level of lead and mercury depicts the potential of novel selective cation transport membranes for decontamination of water on industrial scale.

Table 2 Porosity of PCS-*g*-DA and PCS-*g*-DA/AuNPs-PSNPs membranes in different solvents.

Concentration	Porosity (g/cm^2)			
	Water	Ethanol	Methanol	Propanol
PCS-g-DA	0.11	0.09	0.08	0.05
PCS-g-DA/AuNPs-PSNPs 0.1	0.15	0.10	0.09	0.07
PCS-g-DA/AuNPs-PSNPs 0.3	0.19	0.12	0.12	0.08
PCS-g-DA/AuNPs-PSNPs 0.5	0.24	0.15	0.13	0.09
PCS-g-DA/AuNPs-PSNPs 1	0.29	1.17	0.16	0.14

Table 3 % Solvent content of PCS-*g*-DA and PCS-*g*-DA/AuNPs-PSNPs membranes in different solvents.

Concentration	Water	Ethanol	Methanol	Propanol
PCS-g-DA	1.13	0.99	0.87	0.44
PCS-g-DA/AuNPs-PSNPs 0.1	2.34	0.15	0.11	0.67
PCS-g-DA/AuNPs-PSNPs 0.3	2.47	1.22	0.18	0.78
PCS-g-DA/AuNPs-PSNPs 0.5	2.56	1.45	1.23	0.89
PCS-g-DA/AuNPs-PSNPs 1	3.17	1.67	1.77	0.92

Table 4 Shrinkage ratio of PCS-*g*-DA and PCS-*g*-DA/AuNPs-PSNPs membranes in different solvents.

Concentration	Water	Ethanol	Methanol	Propanol
PCS-g-DA	10.2	8.15	7.25	6.90
PCS-g-DA/AuNPs-PSNPs 0.1	9.82	7.33	7.04	5.56
PCS-g-DA/AuNPs-PSNPs 0.3	9.11	6.98	6.77	5.23
PCS-g-DA/AuNPs-PSNPs 0.5	8.66	6.56	6.56	5.03
PCS-g-DA/AuNPs-PSNPs 1	8.12	6.14	6.32	4.88

Table 5 Pure water flux, salt rejection, recovery of PCS-*g*-DA and PCS-*g*-DA/AuNPs-PSNPs membranes.

Membrane type	Pure water flux (mLcm^{-2} min^{-1})	Salt rejection (%)	Recovery (%)
PCS-g-DA	14.2	45.2	75.2
PCS-g-DA/AuNPs-PSNPs 0.1	14.9	52.7	76.5
PCS-g-DA/AuNPs-PSNPs 0.3	15.7	65.3	80.2
PCS-g-DA/AuNPs-PSNPs 0.5	16.2	68.4	85.1
PCS-g-DA/AuNPs-PSNPs 1	17.4	72.2	87.2

Table 6 Solid–liquid extraction of various metal cations from aqueous solution by PCS-*g*-DA and PCS-*g*-DA/AuNPs-PSNPs 1.

Salt	%E		Kd′/L mol^{-1}		α ×10^3	
	PCS-*g*-DA	PCS-*g*-DA/AuNPs-PSNPs 1	PCS-*g*-DA	PCS-*g*-DA/AuNPs-PSNPs 1	PCS-*g*-DA	PCS-*g*-DA/AuNPs-PSNPs 1
$Fe(NO_3)_3$	31	37	17	25	8	9
$Cu(NO_3)_2$	34	67	19	93	9	1×10^1
$Co(NO_3)_2$	34	67	19	93	9	1×10^1
$Cd(NO_3)_2$	35	67	19	93	9	1×10^1
$Ni(NO_3)_2$	35	67	19	93	9	1×10^1
$Pb(NO_3)_2$	99	99	30×10^2	30×10^2	1×10^3	1×10^3
$Hg(NO_3)_2$	99	99	30×10^2	30×10^2	1×10^3	1×10^3

3.5. Analysis of glass transition temperature

The glass transition of the membranes was studied using DSC. As shown in Fig. 7, the glass-transition temperature of matrix increased with AuNPs-PSNPs loading. The segmental T_g was recorded in the range of 115-151 ℃. The PCS-g-DA/AuNPs-PSNPs 0.1, PCS-g-DA/AuNPs-PSNPs 0.3, PCS-g-DA/AuNPs-PSNPs 0.5 and PCS-g-DA/AuNPs-PSNPs 1 showed glass transition temperature of 115, 128, 135, and 151 ℃ respectively. On the other hand neat PCS-g-DA matrix revealed lower glass transition temperature of 99 ℃. The DSC curves also showed clear shift towards higher temperature with the inclusion of higher nanofiller content. The higher glass transition for the membrane with higher AuNPs-PSNPs nanoparticle content depicted increase in structural rigidity of PCS-g-DA matrix.

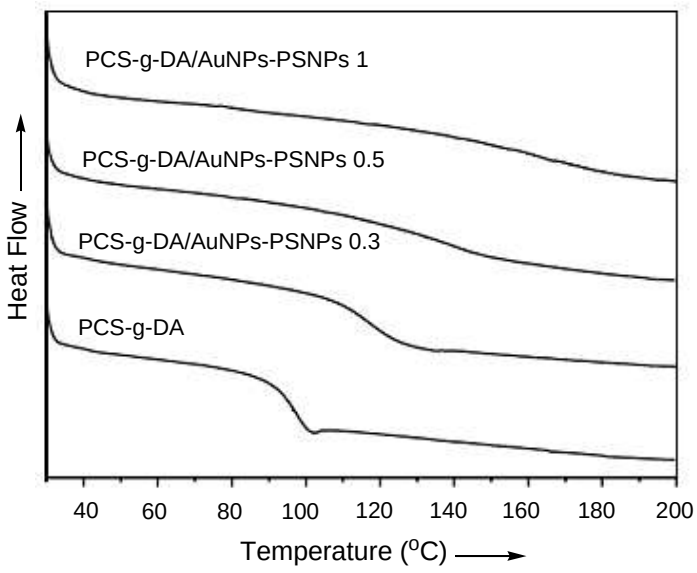

Figure 7 DSC curves of PCS-*g*-DA with varied AuNPs-PSNPs content.

4. Conclusion

The cross-linked poly(4-chlorostyrene) was prepared through solution polymerization. The spherical gold/polystyrene nanoparticles have the size of 30-50 nm. The composite nanoparticles acted as good reinforcement for PCS-g-DA matrix. The mechanical properties of hybrids were improved considerably with the increase in nanofiller loading. Particularly for 1 wt. % loaded PCS-g-DA/AuNPs-PSNPs 1, the cross-linked polystyrene had good compatibility and formed strong interaction with the nanoparticles. As a distinguishing advantage of the polymeric fillers, the glass transition of AuNPs-PSNPs-filled membranes was found higher than the pristine matrix. The nanoporous morphology of the membranes was observed and nanoparticles showed the entire embedding character. Moreover the PCS-g-DA/AuNPs-PSNPs 1 membrane showed better efficiency for the removal of Pb^{2+} and Hg^{2+} from water. The excellent properties such as porosity, flux, shrinkage ratio, recovery, and rejection revealed that the novel membranes can be employed in large scale water purification set-up.

5. References

1. Abdallah H, El-Gendi A, El-Zanati E, Matsuura T. Pervaporation of methanol from methylacetate mixture using polyamide-6 membrane. ***Desal Wat Treat.*** 2013, 51: 7807-7814
2. Aparaschivei R, Şunel V, Popa M, Desbrieres J. Sulfonic Derivatives of 2-Mercaptobenzoxazole and Its Conjugates with Poly(Maleic anhydride-alt-vinyl acetate) with Potential Pharmacological Applications. ***Int J Polym Mater.*** 2014, 63: 268-276
3. Alayemieka E, Lee S. Modification of polyamide membrane surface with chlorine dioxide solutions of differing pH. *Desal Wat Treat.* 2013, 45: 84-90
4. Phillip W A, Hillmyer M A, Cussler E L. Cylinder Orientation Mechanism in Block Copolymer Thin Films Upon Solvent Evaporation. *Macromolecules.* 2014, 43: 7763-7770
5. Kiran K, Goswami S. PMMA/PHEA Interpenetrating Network Embedded With Iron Oxide Nanoparticles for Drug Delivery Applications. *Int J Polym Mater.* 2014, 63: 963-970
6. Tagliazucchi M, Azzaroni O, Szleifer I. Responsive Polymers End-Tethered in Solid-State Nanochannels: When Nanoconfinement Really Matters. *J Am Chem Soc.* 2014, 132: 12404-12411.
7. Mehta A, Zydney A L. Permeability and selectivity analysis for ultrafiltration membranes. *J Membr Sci.* 2005, 249: 245-249
8. Said M M, El-Aassar A H M, Kotp Y H, Shawky H A, Abdel Mottaleb M S A. Performance assessment of prepared polyamide thin film composite membrane for desalination of saline groundwater at Mersa Alam-Ras Banas, Red Sea Coast, Egypt. ***Desal Wat Treat.*** 2013, 51: 4927-4937.
9. Vandezande P, Gevers L E M, Vankelecom I F J. Solvent resistant nanofiltration: separating on a molecular level. ***Chem Soc Rev.*** 2008, 37: 365-405.
10. Petersen R J. Composite reverse osmosis and nanofiltration membranes. ***J Membr Sci.*** 1993, 83: 81-150.
11. Mohan D J, Kullová L. A study on the relationship between preparation condition and properties/performance of polyamide TFC membrane by IR, DSC, TGA, and SEM techniques. ***Desal Wat Treat.*** 2013, 51: 586-596

12. Sandín R, Ferrero E, Repollés C, Navea S, Bacardit J, Espinós J P, Malfeito J J. Reverse osmosis membranes oxidation by hypochlorite and chlorine dioxide: spectroscopic techniques vs. Fujiwara test. ***Desal Wat Treat.*** 2013, 51: 318-327
13. Yanagishita H, Arai J, Sandoh T, Negishi H, Kitamoto D, Ikegami T, Haraya K, Idemoto Y, Koura N. Preparation of polyimide composite membranes grafted by electron beam irradiation. ***J Membr Sci.*** 2004, 232: 93-98
14. A. M. Balachandra, G. L. Baker1, M. L. Bruening, Preparation of composite membranes by atom transfer radical polymerization initiated from a porous support. ***Membr Sci.*** 2003, 227: 1-14
15. Pei G, Chenga G, Du Q. Preparation of chelating resin filled composite membranes, and selective adsorption of Cu(II). ***J Membr Sci.*** 2002, 196: 85-93
16. Wei Y -M, Xu, Z -L, Qusay F A, Wu K. Polyvinyl Alcohol/Polysulfone (PVA/PSF) Hollow Fiber Composite Membranes for Pervaporation Separation of Ethanol/Water Solution. ***J Appl Polym Sci.*** 2005, 98: 247-254
17. Liu J, Su Y, Peng J, Zhao X, Zhang Y, Dong Y, Jiang Z. Preparation and Performance of Antifouling PVC/CPVC Blend Ultrafiltration Membranes. ***Ind Eng Chem Res.*** 2012, 51: 8308-8314
18. Bagheripour E, Moghadassi A R, Hosseini S M. Novel nanofiltration membrane with low concentration of polyvinylchloride: Investigation of solvents' mixing ratio effect (Dimethyl acetamide/Tetrahydrofuran). ***Arab J Chem.*** 2014, DOI: 10.1016/j.arabjc.2014.01.019
19. Slocik J M, Zabinski Jr. J S, Phillips D M, Naik R R. Colorimetric response of peptide-functionalized gold nanoparticles to metal ions, ***Small.*** 2008, 4: 548-551
20. San-Jose N, Gomez-Valdemoro A, García F, Calderon V, García J M. Novel aliphatic–aromatic poly(amide urea)s: synthesis, characterization and application to the elimination of environmentally toxic heavy metal ions, ***React Funct Polym.*** 2008, 68: 1337-1345
21. Wu Y, Zhang Y, Xu J, Chen M, Wu L. One-step preparation of PS/TiO_2 nanocomposite particles via miniemulsion polymerization. ***J Colloid Interfac Sci.*** 2010, 343: 18-24
22. Kausar A, Hussain S T. Investigation of physical properties and structure–property relationship in new poly(azo-sulfone-amide)s. ***High Perform Polym.*** 2013, 25: 387-398
23. Buonomennaa M G, Macchib P, Davolic M, Driolia E. Poly(vinylidene fluoride) membranes by phase inversion: the role the casting and coagulation conditions play in their morphology, crystalline structure and properties. ***Eur Polym J.*** 2007, 43: 1557-1572
24. Ashraf R, Kausar A, Siddiq M. High-performance polymer/nanodiamond composites: synthesis and properties. ***Iran Polym J.*** 2014, 23: 531-545
25. Jing M, Lingling L, Guohua C, Congjie G, Shengxiong D. Preparation of N, O-carboxymethyl chitosan (NOCC) composite nanofiltration membranes and its rejection performance for the fermentation effluent from a wine factory. ***Chin J Chem Eng.*** 2008, 16: 209-213
26. Kausar A, Hussain S T. New generation of thermally stable and conducting poly(azomethine-ester)s: nano-blend formation with polyaniline. 2013, 62: 1442-1450
27. Kausar A, Hussain S T. Synthesis and properties of poly(thiourea-azo-naphthyl)/multi-walled carbon nanotube composites. ***J Plast Film Sheet.*** 2014, **30:** 205-224
28. Duhart A, Dozol J F, Rouquette H, Deratani A. Selective removal of cesium from model nuclear waste solutions using a solid membrane composed of an unsymmetrical calix[4]arenebiscrown-6 bonded to an immobilized polysiloxane backbone. ***J Membr Sci.*** 2001, 185: 145-155

29. Calderón V, Serna F, García F, de la Peña J L, García J M. Selective solid–liquid extraction of cations using solid-phase polyamides with crown ether moieties as cation host units. ***J Appl Polym Sci.*** 2007, 106: 2875-2884.